Thickness Measurement of a Transparent Thin Film Using Phase Change in White-Light Phase-Shift Interferometry

Jaeho Kim[1], Kwangrak Kim[2], and Heui Jae Pahk[1]*

[1]*School of Mechanical and Aerospace Engineering, Seoul National University,
Gwanak-ro 1, Gwanak-gu, Seoul 08826, Korea*
[2]*SNU Precision Co., Ltd., Asan valley nam-ro 124, Dunpo-myeon, Asan-si, Chungcheongnam-do 31409, Korea*

Measuring the thickness of thin films is strongly required in the display industry. In recent years, as the size of a pattern has become smaller, the substrate has become larger. Consequently, measuring the thickness of the thin film over a wide area with low spatial sampling size has become a key technique of manufacturing-yield management. Interferometry is a well-known metrology technique that offers low spatial sampling size and the ability to measure a wide area; however, there are some limitations in measuring the thickness of the thin film. This paper proposes a method to calculate the thickness of the thin film in the following two steps: first, pre-estimation of the thickness with the phase at the peak position of the interferogram at the bottom surface of the thin film, using white-light phase-shift interferometry; second, accurate correction of the measurement by fitting the interferogram with the theoretical pattern through the estimated thickness. Feasibility and accuracy of the method has been verified by comparing measured values of photoresist pattern samples, manufactured with the halftone display process, to those measured by AFM. As a result, an area of 880 × 640 pixels could be measured in 3 seconds, with a measurement error of less than 12%.

Keywords : Thickness, Phase extraction, Thin film, Interferometry, Interferogram modeling
OCIS codes : (120.0120) Instrumentation, measurement, and metrology; (120,3180) Interferometry;
(120.3940) Metrology

I. INTRODUCTION

Thickness measurement of thin films is required in various industries, and is exceptionally important in the display industry. Currently the display industry is rapidly moving from LCD to OLED technology, and, as a result, precise manufacturing of thin films has become a key factor in improving display quality and increasing production yield. Accordingly, techniques for accurately measuring and examining the thickness distribution of a pattern have become important. Furthermore, as the display tends to have higher resolution and the size of the panel increases, the pattern becomes smaller, while the area of inspection increases. As a result, the importance of thin-film measurement techniques over a large area with low spatial sampling

receives more attention.

In general, interferometry is used to measure surface shape, including thin-film thickness [1]. It is a powerful means to measure a surface using light's interference phenomenon. The thickness can be measured by the phase difference of the interferograms generated on the upper and lower surfaces of the thin film [2]. When the film is very thin, however, it is difficult to acquire the phase, because the two interferograms overlap completely.

A number of studies have been conducted to measure thickness using spectrally resolved white-light interferometry (SRI) [3-6]. SRI calculates the height and thickness of the sample using phase data, which is obtained by sweeping the wavelength of the white-light source. SRI also has the weakness that its accuracy may be low, due to its

---

*Corresponding author: hjpahk@snu.ac.kr

Color versions of one or more of the figures in this paper are available online.

sensitivity to focus change along the z axis. Studies have also been carried out to measure thickness using frequency analysis of the interferogram. Frequency-domain processing, including fast Fourier transform (FFT) [7] and wavelet transform [8], has been advanced to derive the phase of interferogram, and has eventually allowed one to simultaneously calculate the surface and thickness of a thin film by fitting the theoretically modeled phases. A method using the helical conjugate function (HCF) was also studied [9-11]. It measures thickness in a similar way to spectroscopic analysis, which obtains the wavelength spectrum through the frequency-domain conversion of the interferogram using white-light phase-shift interferometry (WLPSI). However, due to the sensitivity of signals in the frequency domain, that method is vulnerable to the slightest noise, such as external noise on the raw interferogram data. There is another report that used both interferometry and spectroscopic reflectometry (SR) to measure thickness and surface dimensions [12-14]. However, the efficiency of the method is questionable, because of its redundancy in using multiple instruments, and relatively slow processing time for the two-step measurement.

This paper proposes a new method to measure the thickness using only WLPSI. It exploits the phenomenon in which the phase at the peak position of interferogram at the bottom of a thin film, relative to that at the substrate, shifts according to the change of thickness. This paper shows the derivations of the phase-thickness relation and the estimate of thickness using the phase of the measured interferogram. Ambiguity due to the nonlinearity of the phase-thickness relationship has been overcome by fitting the interferogram. The newly proposed method allows the thickness measurement of a thin-film sample over a large area with low spatial sampling.

II. METHOD OF MEASURING THICKNESS THROUGH THE PHASE OF AN INTERFEROGRAM

2.1. Interferogram Modeling of a Thin-film Sample

Figure 1 shows a schematic diagram of general interferometry. Interferometry uses the interference of two light beams to obtain the phase of the resulting interferogram, and measures the distance to the object. When measuring a sample of thin film, the light intensity of the two beams combined in the interferometry is generally expressed as

$$I(z, k) = |E_r(z, k) + E_t(z, k)|^2 \tag{1}$$

$$E_r(z, k) = E_i \rho(1-\rho)|R_{ref}(k)|^* e^{-i(2kl-\psi_{ref})} \tag{2}$$

$$E_t(z, k) = E_i \rho(1-\rho)|R_{obj}(k)|^* e^{-i(2k(l+h-z)-\psi_{obj})} \tag{3}$$

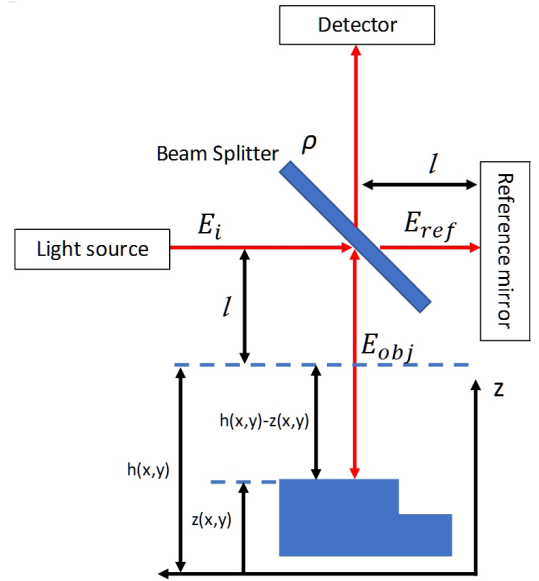where E_r is the wave function of the light reflected from

FIG. 1. Schematic diagram of interferometry.

the reference mirror, E_t is the wave function of the light reflected from the sample, E_i is the wave function of the incident light, ρ is the transmittance of the beam splitter. k refers to the wave number and is represented by $\frac{2\pi}{\lambda}$, R_{ref} and R_{obj} are the total reflection coefficient of reference mirror and sample respectively, ψ_{ref} and ψ_{obj} represent the initial phase of the reference mirror and sample, l is the distance between the beam splitter and reference mirror, h is the position of the scanner, and z is the height of the sample surface. As a result, the optical path difference of the two beams becomes $h - z$. By substituting Eqs. (2) and (3) into (1), the interference light- intensity equation for monochromatic light can be developed as follows.

$$I(z, k) = I_0[1 + \gamma \cos(2k(h-z) - \triangle\psi)] \tag{4}$$

where γ is the visibility function of the interference signal at a particular wavenumber k, and $\triangle\psi$ is the phase offset between the two beams. If the reference mirror is ideal, R_{ref} is 1 for all wavelengths, and ψ_{ref} is a constant that can be omitted from the periodic function.

$$\triangle\psi = \psi_{ref} - \psi_{obj} = -\psi_{obj} = \tan^{-1}(b/a) \tag{5}$$

in which a and b are the real and imaginary parts of $R_{obj}(R_{obj} = a + bi)$. As a result, $\triangle\psi$ can be represented by the phase of R_{obj}.

Figure 2 shows a multiple-reflection model for light impinging upon a thin-film sample. The light coming out of the sample is the sum of the multiple reflected beams, and the total reflection coefficient of the sample R_{obj} is expressed as follows, according to multiple-reflection theory [15].
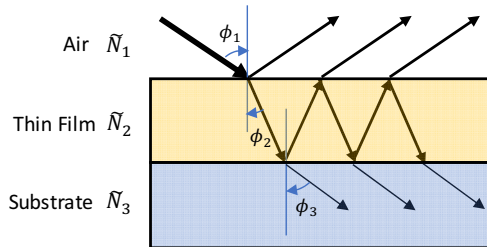
FIG. 2. Schematic diagram of multiply reflected signals.

$$R_{obj} = \frac{r_{12} + r_{23}\exp(-j2\beta)}{1 + r_{12}r_{23}\exp(-j2\beta)} \qquad (6)$$

$$r_{12} = \frac{N_2\cos\varnothing_1 - N_1\cos\varnothing_2}{N_2\cos\varnothing_1 + N_1\cos\varnothing_2} = |r_{12}|\exp(j\delta_{12}) \qquad (7)$$

$$r_{23} = \frac{N_3\cos\varnothing_2 - N_2\cos\varnothing_3}{N_3\cos\varnothing_2 + N_2\cos\varnothing_3} = |r_{23}|\exp(j\delta_{23}) \qquad (8)$$

$$\beta = 2\pi(d/\lambda)N_2\cos\varnothing_2 \qquad (9)$$

Here r_{12} and r_{23} are the Fresnel reflection coefficients of the top and bottom boundaries of the thin film. In general, the Fresnel reflection coefficient is expressed differently for a *p*-wave that is parallel to the incident surface than for an *s*-wave that is perpendicular to the incident surface. However, assuming that the light is normally incident upon the surface, the two equations become the same. As a result, the Fresnel reflection coefficient can be only expressed in a *p*-wave or *s*-wave form; in our case, the *p*-wave expression represents the coefficient. δ_{12}, δ_{23} are the phase changes where reflection occurs at the interfaces of top and bottom boundaries of the thin film respectively. β represents the equation for the phase change of light when it passes through the thin film. d is thickness of the thin film, N_1 and, N_2 and N_3 are the complex refractive indices of air, thin film, and substrate respectively. $\varnothing_1$ is the angle of incidence to the thin film, and $\varnothing_2$ and $\varnothing_3$ are the angles of refraction in the thin film and substrate.

Among the many interferometers, the WLPSI type is used in this paper. Although it has a short coherence length, it uses white light, the mix of all wavelengths throughout the visible region, to eliminate the phase ambiguity that can occur in with a single-wavelength interferometer. Therefore, the light intensity of the WLPSI can be expressed as the sum of the light-intensity components of all wavelengths, as follows.

$$I(z, k) = \int_{k_1}^{k_2} I_0[1 + \gamma\cos(2k(h-z) - \triangle\psi)] * F(k)dk \qquad (10)$$

k_1 and k_2 are the starting and ending wave numbers of the white-light-source spectrum used in the interferometer, and $F(k)$ is the spectrum of the light source, according to wave number.

The interferogram according to the thickness of thin film can be modeled by the equations above. Figure 3 shows the result of modeling the change in the interferogram as the thickness of SiO_2 (deposited on Si of constant height) is varied. When the film is very thin, the interferograms of the thin film at the top boundary (where the light enters from ambient atmosphere into SiO_2) and the bottom boundary (where the light exits the SiO_2 and enters the Si) almost overlap, and the signals almost merge into one. The two signals gradually separate as the film of SiO_2 becomes thicker. In this case the most significant factor for measuring the thickness of the thin film is the interferogram at the bottom boundary: Since the SiO_2 is deposited upon a constant height of Si, the bottom interference signal generated on the Si surface is easily presumed to be in a constant position. However, when the SiO_2 film grows, not only does the position of the top-boundary signal change, but also the bottom-boundary signal moves. The peak point on the interferogram at the bottom boundary is represented by the cosine integral including the $\triangle\psi$ term. $\triangle\psi$ is the phase of total reflection coefficients of the sample R_{obj}, R_{obj} which varies with the thickness of the film. As a result, the phase at the interferogram peak along the z axis is influenced by the thickness variation, and the thickness can be estimated through the phase at the peak point. The change in location of the bottom-boundary signal can be found in both simulations and experimental datasets, which will be presented in the following sections.

(a)

(b)

(c)
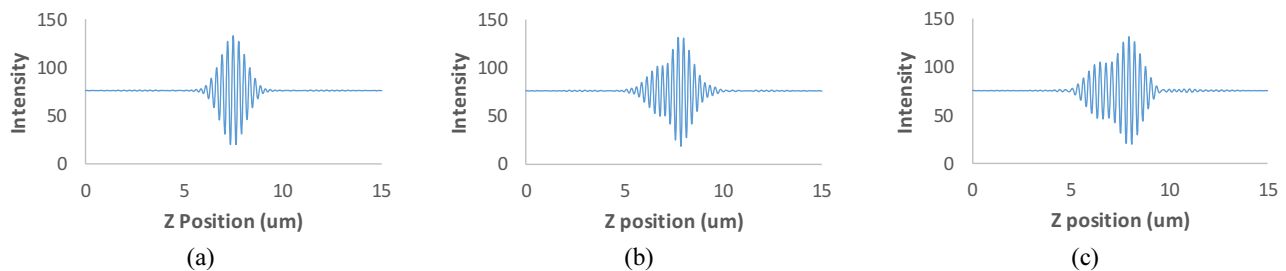
FIG. 3. Interferogram modeling results for Si/SiO_2 samples with varying SiO_2 thickness: (a) no film; (b) 500 nm SiO_2; (c) 1000 nm SiO_2.

2.2. Derivation of the Phase-thickness Relation in the Interferogram

With this in mind, we try to model the phase change at the peak position of the interferogram at the bottom boundary, as the film thickness changes. First, the visibility function of the interferogram is extracted, and the vertex of the visibility function is calculated. We use the method proposed by Larkin to extract the visibility function of the interferogram [16]. It can be obtained with light intensities adjacent to the intensity at the reference position.

$$M = \frac{(I_{-1} - I_1)^2 \left\{ [4(I_{-1} - I_1)^2 - (I_{-2} - I_2)^2] + (-I_{-2} + 2I_0 - I_2)^2 \right\}^{\frac{1}{2}}}{4(I_{-1} - I_1)^2 - (I_{-2} - I_2)^2} \tag{11}$$

M is the visibility function of the white-light interference signal, which represents the envelope of the interferogram. The square of the visibility function can also be expressed by a simpler formula,

$$M^2 \propto (I_{-1} - I_1)^2 - (I_{-2} - I_0)(I_0 - I_2) \tag{12}$$

where I_{-2}, I_{-1}, I_0, I_1, and I_2 are successive, adjacent light intensities, and I_0 is the light intensity at the reference position, which is the center of the function calculation. It is assumed that the light-intensity scanning is performed with an interval of $1/4$ λ (phase of $1/2$ π) to calculate the complete phase, according to the Nyquist theorem [17].

Figure 4 shows the visibility function of the interferogram, extracted by Larkin's method (Fig. 3). The movement of the interferogram with the change in film thickness is clearly observed. From the vertices of the visibility function, the phase at the peak of the visibility function can be obtained as follows.

$$\varnothing_{wsi} = \frac{z_{peak\ of\ visibility\ function} * 1}{2} \pi \tag{13}$$

After obtaining the position and phase of the peak of the visibility function, the phase vertices of the fringes are obtained by using the 5-bucket algorithm [18] and intensities adjacent to the intensity at the peak of the visibility function. The formulas for each light intensity, when obtaining two points on either side of the intensity at the peak of the visibility function, are as follows.

$$\begin{aligned}
I_{-2} &= I_0[1 + \gamma \cos(\varnothing_{-2})] \\
I_{-1} &= I_0[1 + \gamma \cos(\varnothing_{-1})] \\
I_0 &= I_0[1 + \gamma \cos(\varnothing_0)] \\
I_1 &= I_0[1 + \gamma \cos(\varnothing_1)] \\
I_2 &= I_0[1 + \gamma \cos(\varnothing_2)]
\end{aligned} \tag{14}$$

Based on the above equations, the phase vertices of the fringes at the center point I_0 can be obtained from the following equation.

$$\varnothing_{0,psi} = \tan^{-1} \left\{ \frac{2(I_{-1} - I_1)}{2I_0 - I_{-2} - I_2} \right\} \tag{15}$$

As a result, we can obtain the phase of the WLPSI by using the phase at vertex of the visibility function and the phase vertices of the fringes

$$\varnothing_{wlpsi} = \varnothing_{wsi} + \varnothing_{psi} \tag{16}$$

Using Eq. (10), we can model the interferogram according to the film thickness and extract the phase at the peak position of the interferogram at bottom boundary, from the previous principle. Finally, the relation between thin-film thickness and phase at the peak position of the lower interference signal is shown in Fig. 5. It was simulated for the two material systems Si/SiO_2 and Mo/Photoresist (PR), per the conditions of the samples to be measured in experiments. Since the phase is set to zero when the thin film is not present, the phase shown in this paper should be considered as the *relative* phase to that of the substrate without thin film.
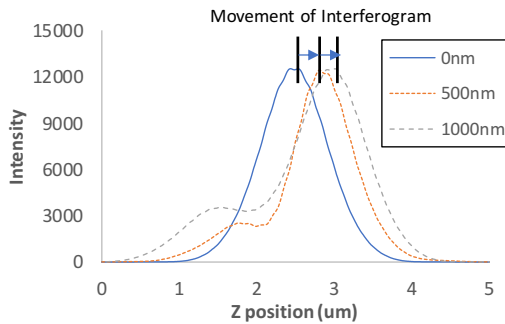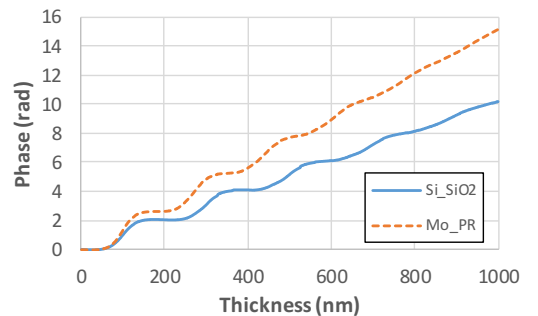

FIG. 4. Change in visibility function according to SiO_2 thickness in a Si/SiO_2 sample, calculated by Larkin's method, and modulus peak shifts as the thin-film thickness changes.

FIG. 5. The change of WLPSI phase due to thin-film thickness for Si/SiO_2 and Mo/PR. It is possible to confirm that the tendency of the phase change depends on the material.

2.3. Nonlinear Fitting to Remove Ambiguity

In Fig. 5, the graph shows that there is a correlation between the thickness and the phase at the peak position of the bottom-boundary interferogram, even though it is not perfectly linear. As a result, it seems that the approximate thickness of the film can be deduced from the relative phase of the substrate and the thin film at the bottom boundary.

When the phases of the interferograms at the bottom boundary over a surface region are obtained for different thicknesses as described above, the thickness of the thin film can be measured through the relationship between phase and thickness. However, since the relationship between the two is not completely linear, an additional step is needed to enhance accuracy. For this process, the interferogram-modeling Eq. (10) for the thin-film sample is used again. The thickness can be calculated by fitting the theoretically modeled interferogram to the interferogram obtained by actual measurement. We employ the Levenberg-Marquardt nonlinear fitting technique, which uses the following error function:

$$e(d, h) = \sum_{Scanstart}^{Scanend} \left(I_{Measured}(z) - I_{Theory}(z:d,h) \right)^2 \quad (17)$$

The above nonlinear fitting for scaling correction should be performed throughout the entire scan region; however, if the thickness throughout the area is consistent, it may be performed only once. In previous cases, the method of modeling and fitting the interferogram had the disadvantage of taking a long time as the search range of the fitting variable increases, and the accuracy of the fitting could be reduced because of easy convergence to a local minimum [14]. However, by using the proposed method, the thickness can be quickly calculated with a small fitting range which is primarily narrowed down to
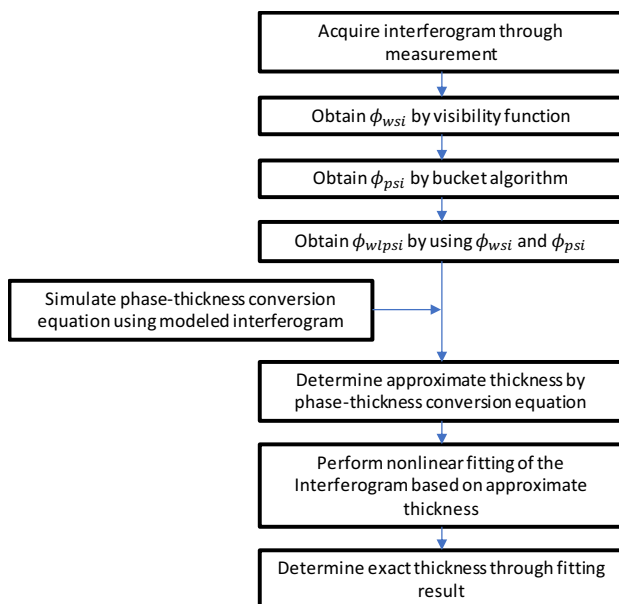
the true value by using the phase of interferogram.

Ultimately, this new method allows one to measure the thickness at high speed using a conventional white-light phase-shift interferometer, without any additional device support. As a result, the overall sequence of the method used in this experiment is shown in Fig. 6.

III. EXPERIMENT

Figure 7 shows the equipment configuration for the experiment to verify the proposed method. A Mirau-type WLPSI is used as the optical system. A 10× interference objective lens (Nikon, CF IC EPI Plan DI 10×) and a 1× tube lens are used to form the image on an area camera. The coaxial illumination of a white-light LED is used as the light source, and a PZT scanner is used to perform the phase scan while moving the lens in the z-axis direction. To obtain the best image from the optical system, only an 880× 640 area is extracted from the camera's CMOS sensor, which actually has 1280×1024 resolution. The images are captured at 75-nm intervals through a 15-μm z-axis scan. Since the size of one pixel of the camera is 4.8×4.8 μm² and a lens with 10× magnification is used, the spatial sampling is 0.48×0.48 μm² and the area of the entire field of view (FOV) is 422.4×307.2 μm².

The sample is a VLSI standard specimen deposited with SiO_2 on Si at a certified thickness of 398 nm. The image of the sample is shown in Fig. 8(a). SiO_2 is deposited in a chevron pattern in the middle region, and the bare silicon surface without thin film is present on both sides of the chevron pattern. Fig. 8(b) shows the result of mapping the phase from the WLPSI to the whole region by the method shown in the previous chapter. It can be seen that the

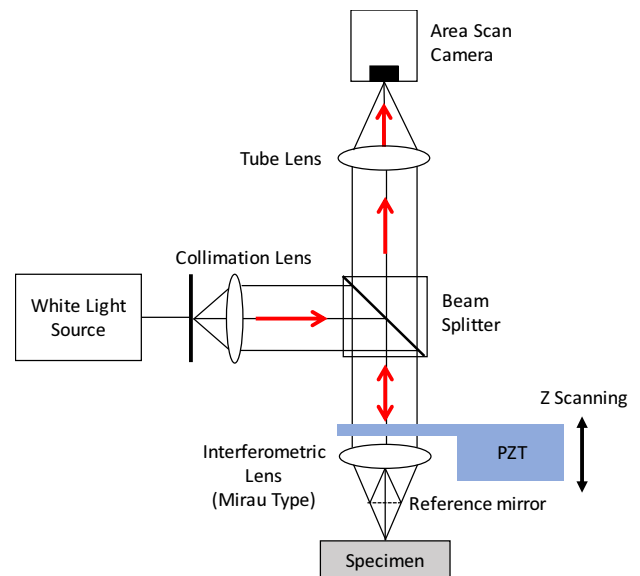FIG. 6. A flowchart for the entire method.

FIG. 7. The optical system used in this experiment. WLPSI is used with a white-light LED source and a Mirau-type lens.
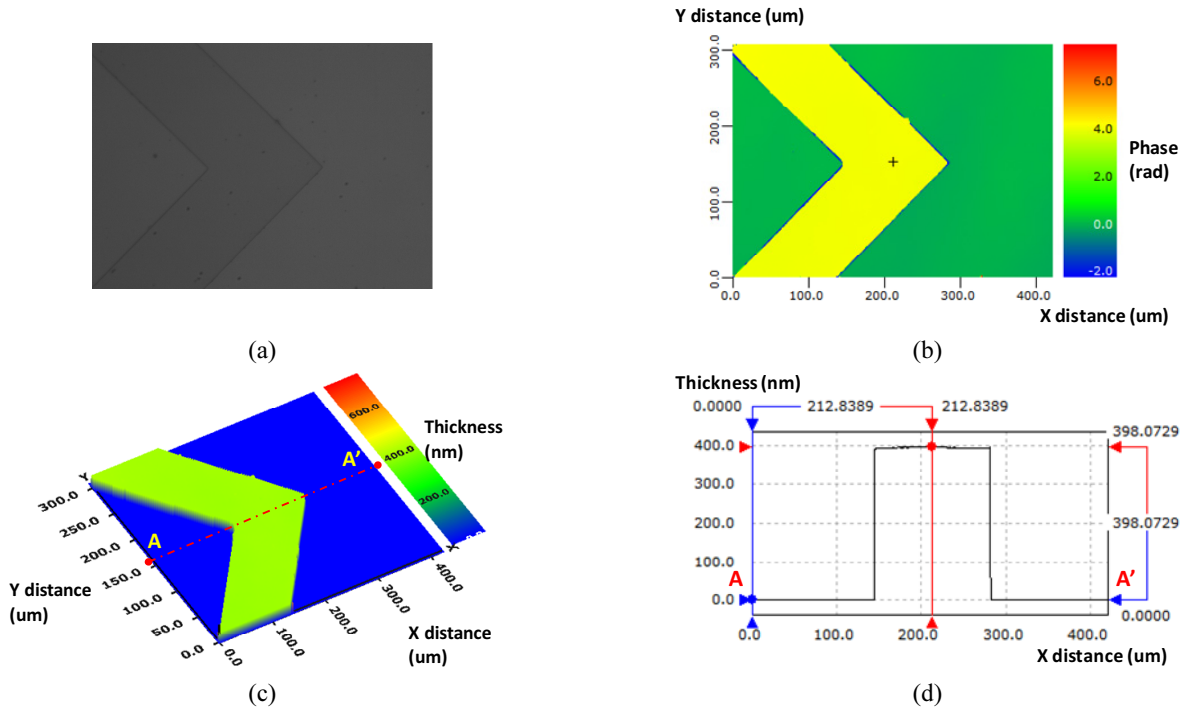
FIG. 8. Measurement results for Si/SiO_2 standard samples: (a) Image of the sample; (b) Results from WLPSI phase extraction; (c) Three-dimensional shape of the measured thickness; (d) Horizontal section (A-A') profile of the measurement result.

phase of the SiO_2 thin film is different significantly from that of the bare silicon surface. The thickness is calculated from the obtained phase using the phase-thickness relation derived in the previous chapter. We then conduct nonlinear fitting with thickness as the fitting variable, using the interferogram-modeling equation to accurately determine the scale of the thickness-phase relationship, which could be ambiguous due to nonlinearity. Fig. 8(d) shows the profile section of the final thickness. The thickness results are consistent with the VLSI certificate values. As a result, it is confirmed that the thickness measurement using the proposed algorithm is effective. It takes under 3 seconds to measure the thickness of the large area.

Next, a photoresist (PR) pattern sample, as is widely produced in the halftone process of the display industry, is measured. In the halftone process a thick PR and a thin PR are deposited at once, to reduce the number of lithography processes. Knowing the exact thickness of the PR is a key component of process control. The PR is deposited on the metal surface that is used as the electrode. Since the thickness of thin PR gradually increases and decreases along the channel formed in the gap between two thick PR sections, there is a continuous thin film with varying thickness in this sample. Figure 9(a) shows the shape of the halftone sample used in this experiment. Two sections of thick PR are deposited on a molybdenum surface, and thin PR is deposited between the two thick photoresists. The measurement is performed only for the thin PR-patterned area, as indicated by the dotted rectangle.

The thick PR area is not experimented upon, because it is thick enough to be accurately measured even by conventional interferometry. Unlike for the VLSI standard specimen, here a 50× interference lens (Nikon, CF IC EPI Plan DI 50×) is used, due to the pattern size. The spatial sampling is 0.098 × 0.098 μm^2, which is smaller than in the previous experiment, and the total area of the FOV is 45.08 × 5.88 μm^2, since the number of pixels in the dotted area is 460 × 60.

The results of the thickness measurements are shown in Fig. 9(b). To verify the accuracy of the data, measurements were also conducted using an atomic force microscope (AFM) (Fig. 9(c)). The result of the proposed method gives the same height as measured by AFM, and also the height profiles of the sample from both AFM and the proposed method match. Figure 10 compares the measurements by WLPSI and AFM by layering the same cross-sectional profiles. This confirms the accuracy of the method used in this experiment. Table 1 compares the results measured by AFM to those by the proposed method in the PR sample examined in this experiment. According to the errors from this comparison, the samples of height 400 nm or greater have a relatively low error, under ±3.8%, but samples of thickness less than 400 nm yield a relatively high error, up to 12%. The reason for relatively low accuracy at low thicknesses is that low-thickness points are located on an inclined surface, which has gradually increasing height, whereas the high-thickness points are located on a continuous, flat, and large surface. If all the points were in the flat-plane surface, the low-thickness points would show errors similar to those for the current high-thickness points (< 3.8%).
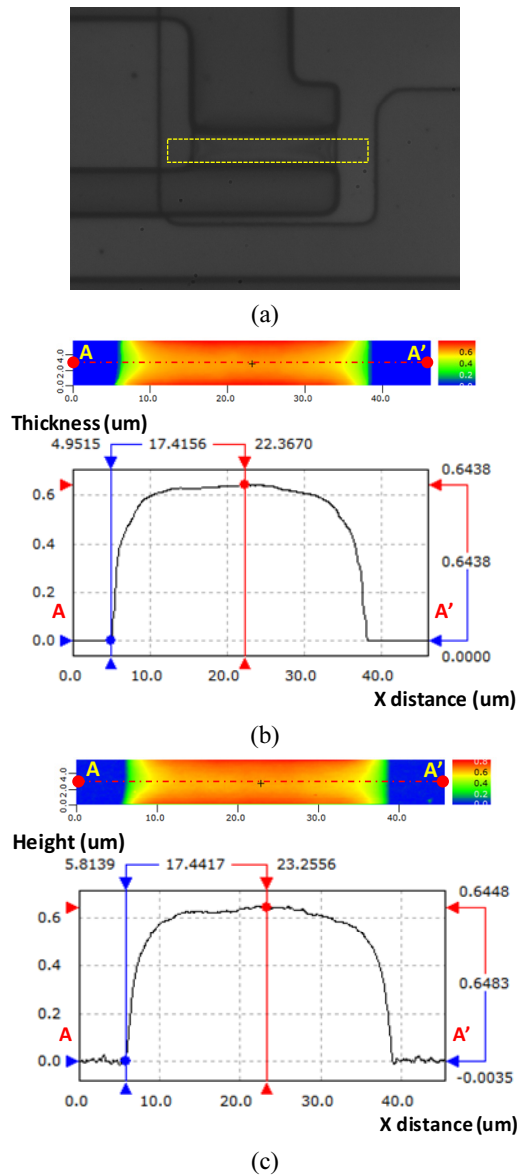
(a)

(b)

(c)

FIG. 9. Measurement result of the PR sample: (a) From the entire sample area, the portion within the yellow dotted line was extracted, and the measurement was performed; (b) The results measured by the proposed method; (c) A measurement over the same section is acquired by AFM.
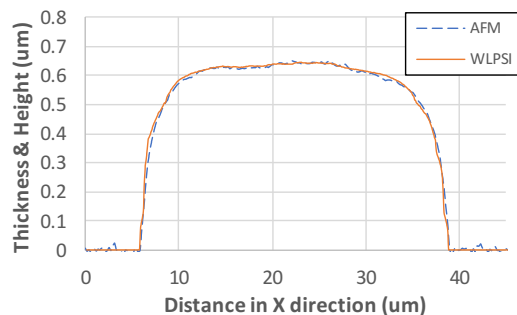

FIG. 10. Comparison of data measured by the proposed method to those measured by AFM for the same cross section.

TABLE 1. Comparison of measured results from AFM and the proposed method, conducted on the same PR samples at points with various thicknesses

Unit: nm	AFM	Proposed method	Error (%)
Point 1	50	56	12
Point 2	100	91	-9
Point 3	200	181	-9.5
Point 4	300	326	8.7
Point 5	400	414	3.5
Point 6	500	496	-0.8
Point 7	600	607	1.2

IV. DISCUSSION

There are many sources of phase error, but generally it occurs when external vibration exists, and when the surface is highly inclined, such that it forms a steep edge. To avoid phase error and accurately obtain the phase for any surface, the unwrapping method is used. The phase error is eliminated by comparing the data with those for neighboring pixels [19, 20]. Figure 11 is a graph showing the difference in phase results with and without this correction. Without phase correction, the signal contains phase-jumping data, especially on the steep edge of the PR sample. The proposed method can be made more stable through use of this phase-correction algorithm.

The existing limitations of conventional thickness-measurement methods based on interferometry is that they can only measure thick films. If the thickness of the film is 100 nm or less, conventional measurement methods are unreliable. [7, 14]. However, the proposed method enables one to measure the thin-film thicknesses under 100 nm. Figure 12 shows a graph comparing the true thickness values of the sample with the thickness that is actually measured using the proposed methods. It shows that the accuracy of the measurement remains good, even for samples thinner than 100 nm.
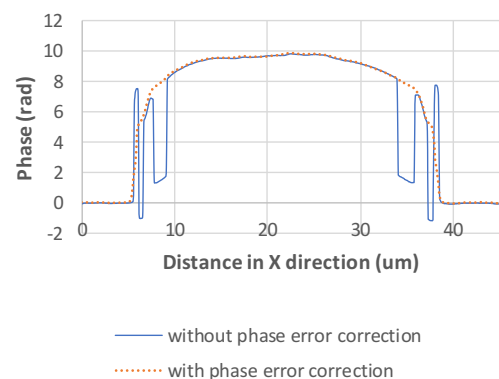

FIG. 11. Result of phase calculation, with or without phase correction, for the PR sample.
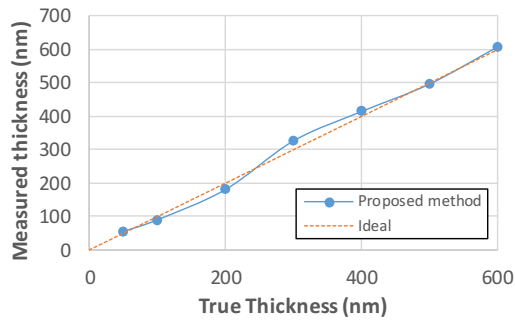
FIG. 12. Comparison of true data to data measured by the proposed method, for points with various thicknesses.
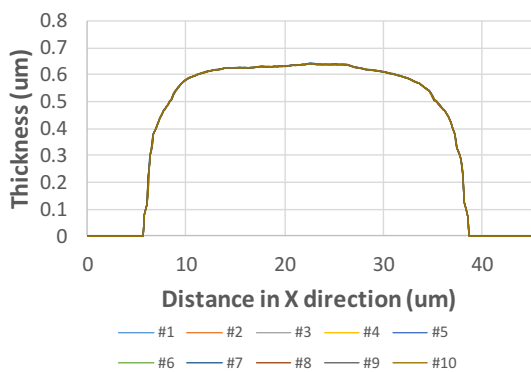

FIG. 13. Profiles of repeated-measurement data using the proposed method, showing that the 10 profiles almost entirely overlap.

So far, the results of a *single* measurement have been presented. We also perform a repeated-measurement test, to demonstrate the reproducibility and repeatability of the proposed method. This is performed after some time interval, following the previous single-measurement experiments.

The same PR sample is used as in the previous experiment. 10 consecutive measurements are conducted on the sample using WLPSI and the proposed method.

Figure 13 shows the profiles of the repeated measurements. The profiles almost completely overlap, proving the stability of the proposed method. The shapes of the repeated measurements are also consistent with the previous single-measurement profile of Fig. 10. The consistency regardless of measurement time demonstrates the excellent reproducibility. The details of repeated measurement are shown in Table 2. The data in Table 2 are for different points on the sample from the measured point of Table 1. Among the results of all points, the maximum 3σ value was less than 6 nm, showing that the proposed method has good repeatability.

Despite its powerful ability to measure thin films, the proposed method still has some constraints. Since the phase of the thin film at the bottom surface is relative to that of the bare metal substrate, it is necessary to locate the bare substrate within the measurement FOV. As shown in Fig. 9(a), the PR sample that is use in the experiment also has the metal-substrate region within the captured FOV. In addition, the accuracy of the proposed method depends highly on the accuracy of the phase at the bottom surface. Therefore, regardless of its thickness, when the reflectance of the substrate is low or the phase signal of the bottom surface is weak and difficult to detect, the proposed method is inapplicable.

Even with those constraints, we think that this is a powerful means to accurately measure the thickness of a large area, if the prerequisite conditions are met.

V. CONCLUSION

In this paper, using WLPSI, the thickness of a thin film

TABLE 2. Repeated-measurement data using the proposed method for points of various thicknesses (The points are different from those in Table 1)

Unit: nm	Point 1	Point 2	Point 3	Point 4	Point 5	Point 6
Average	59.1	101.0	303.6	402.3	501.7	600.1
3σ	2.2	3.6	5.7	3.3	3.7	2.6
#1	58.7	102.2	301.9	404.2	500.9	599.9
#2	58.3	102.1	305.4	402.0	501.6	600.5
#3	59.3	100.1	301.2	403.3	499.7	600.4
#4	60.2	101.3	304.9	402.9	500.5	598.9
#5	57.8	102.2	304.5	400.7	501.5	599.2
#6	59.2	101.2	304.9	402.0	502.7	601.5
#7	59.2	101.3	303.9	403.0	502.9	600.1
#8	60.1	100.4	302.8	401.4	503.2	601.1
#9	59	98.3	300.5	401.0	500.9	599.0
#10	59.1	100.8	306.1	402.8	503.3	600.6

was measured using the phase of the film at its bottom surface. The significance of the experiment can be summarized as follows.

(1) We have modeled the shifts in relative phase at the peak position, between the interferogram of the substrate and that of the thin film at its bottom surface, in the form of the WLPSI signal according to the thickness variation of the thin film, and we have suggested a method to estimate the thickness through the modeled phase. As a result, it was possible to measure the thickness using the existing instrument, without adding any extra devices.

(2) Ambiguity that can be caused by the nonlinearity of the phase-thickness relationship could be eliminated by obtaining a reliable relative scale factor, through nonlinear fitting between the modeled and actual interferograms.

(3) It has as fast a measurement speed as the conventional WLPSI, and is able to quickly calculate the thickness of an area of 880×640 pixel^2 within 3 seconds.

(4) Compared to reference measurements using AFM, the measurement error was less than 12% for thicknesses of 600 nm or less. A significant improvement in accuracy was achieved for films thinner than 100 nm, which have been difficult to measure with conventional methods.

(5) When the repeated-measurement test was performed using the proposed method, good reproducibility was observed in the profiles of the repeated measurements. Also, when the measured value was observed, the maximum 3σ value was less than 6 nm for the entire thickness range of 600 nm or less. As a result, the repeatability was excellent.

ACKNOWLEDGMENT

REFERENCES

1. P. A. Flourney, R. W. McClure, and G. Wyntjes, "White-light interferometric thickness gauge," Appl. Opt. **11**, 1907-1915 (1972).

2. H. Maruyama, S. Inoue, T. Mitsuyama, M. Ohmi, and M. Haruna, "Low-coherence interferometer system for the simultaneous measurement of refractive index and thickness," Appl. Opt. **41**, 1315-1322 (2002).

3. P. Hlubina, D. Ciprian, J. Lunacek, and M. Lesnak, "Dispersive white-light spectral interferometry with absolute phase retrieval to measure thin film," Opt. Express **14**, 7678-7685 (2006).

4. S. K. Debnath, M. P. Kothiyal, J. Schmit, and P. Hariharan, "Spectrally resolved white- light phase-shifting interference microscopy for thickness profile measurement of transparent thin-film layers on patterned substrates," Opt. Express **14**, 4662-4667 (2006).

5. P. Hlubina, J. Lunacek, and D. Ciprian, "White-light spectral interferometric technique to measure a nonlinear phase function of a thin-film structure," Opt. Commun. **283**, 4877-4881 (2010).

6. Y. S. Ghim and S. W. Kim, "Spectrally resolved white-light interferometry for 3D inspection of a thin-film layer structure," Appl. Opt. **41**, 799-803 (2009).

7. S. W. Kim and G. H. Kim, "Thickness-profile measurement of transparent thin-film layers by white-light scanning interferometry," Appl. Opt. **38**, 5968-5973 (1999).

8. Y. M. Hwang, S. W. Yoon, J. H. Kim, S. Kim, and H. Pahk "Thin-film thickness profile measurement using wavelet transform in wavelength-scanning interferometry," Opt. Lasers Eng. **46**, 179-184 (2008).

9. D. Mansfield, "The distorted helix: thin film extraction from scanning white light interferometry," Proc. SPIE **6186**, 61860O (2006).

10. D. Mansfield, "Extraction of film interface surfaces from scanning white light interferometry," Proc. SPIE **7101**, 797978 (2008).

11. B. Maniscalco, P. M. Kaminski, and J. Walls, "Thin film thickness measurements using scanning white light interferometry," Thin Solid Films **550**, 10-16 (2014).

12. D. S. Kim and S. H. Kim, "Fast thickness profile measurement using a peak detection method based on an acousto-optic tunable filter," Meas. Sci. Technol. **13**, L1-L5 (2002).

13. J. W. You, S. Kim, and D. Kim, "High speed volumetric thickness profile measurement based on full-field wavelength scanning interferometer," Opt. Express **16**, 21022-21031 (2008).

14. T. Jo, K. Kim, S. R. Kim, and H. J. Pahk, "Thickness and surface measurement of transparent thin-film layers using white light scanning interferometry combined with reflectometry," J. Opt. Soc. Korea **18**, 236-243 (2014).

15. H. G. Tompkins and W. A. McGahan, *Spectroscopic ellipsometry and reflectometry: a user's guide*, (John Wiley & Sons INC, New York, 1999), pp. 8-21.

16. K. G. Larkin, "Efficient nonlinear algorithm for envelope detection in white light interferometry," J. Opt. Soc. Am. A. **13**, 832-843 (1996).

17. P. de Groot and L. Deck, "Three-dimensional imaging by sub Nyquist sampling of white -light interferograms," Opt. Lett. **18**, 1462-1464 (1993).

18. J. Schwider, R. Burow, K.-E. Elssner, J. Grzanna, R. Spolaczyk, and K. Merkel, "Digital wave-front measuring interferometry: some systematic error sources," Appl. Opt. **22**, 3421-3432 (1983).

19. K. Itoh, "Analysis of the phase unwrapping problem," Appl. Opt. **21**, 2470-2470 (1982).

20. S. R. Kim, J. H. Kim, and H. J. Pahk, "Fringe-order determination method in white-light phase-shifting interferometry for the compensation of the phase delay and the suppression of excessive phase unwrapping," J. Opt. Soc. Korea **17**, 415-422 (2013).